Cellulose
https://doi.org/10.1007/s10570-022-04482-0

ORIGINAL RESEARCH

Cellulose-g-tetraethylenepentamine dual-function imprinted polymers selectively and effectively adsorb and remove 4-nitrophenol and Cr(VI)

Daning Lang · Xia Xu · Ronglan Wu · Wei Wang · Ming Shi · Ke Jia · Shifei Chen · Jide Wang

Received: 24 November 2021 / Accepted: 9 February 2022

Abstract A cellulosic material has been synthesized that could efficiently and selectively adsorb organic and inorganic contaminants from aqueous solutions without interference from competing adsorption sites. Cellulose-graft-tetraethylenepentamine molecular imprinted polymer (C-TEPA-MIP) was synthesized by using 4-nitrophenol (4-NP) as the template. The C-TEPA-MIP adsorbent could adsorb 4-NP and Cr(VI) simultaneously and selectively, without being affected by the competitive adsorption sites of each of these pollutants. The adsorption of 4-NP was predominantly due to the imprinted sites of 4-NP in C-TEPA-MIP that were located inside of the adsorbent, whereas that of Cr(VI) was primarily due to the amine groups of TEPA found on the surface of the adsorbent. Compared with the non-imprint polymer synthesized without the template, C-TEPA-MIP showed higher selectivity for both 4-NP and Cr(VI) in unitary and binary systems. In addition, C-TEPA-MIP exhibited good stability and recyclability for 4-NP, which makes it a promising candidate material for applications concerning wastewater treatment.

Supplementary Information The online version contains supplementary material available at https://doi.org/10.1007/s10570-022-04482-0.

D. Lang · X. Xu · R. Wu (✉) · M. Shi · K. Jia · S. Chen · J. Wang
Key Laboratory of Oil & Gas Fine Chemicals, School of Chemical Engineering, Xinjiang University, Urumqi 830046, China
e-mail: wuronglan@163.com

X. Xu
School of Pharmaceutical & Environmental Engineering, College of Sichuan Chemical Vocational and Technical, Sichuan 646300, China

W. Wang (✉)
Institute of Chemistry & Center for Pharmacy, University of Bergen, 5020 Bergen, Norway
e-mail: wei.wang@uib.no

Published online: 28 February 2022

Graphical abstract

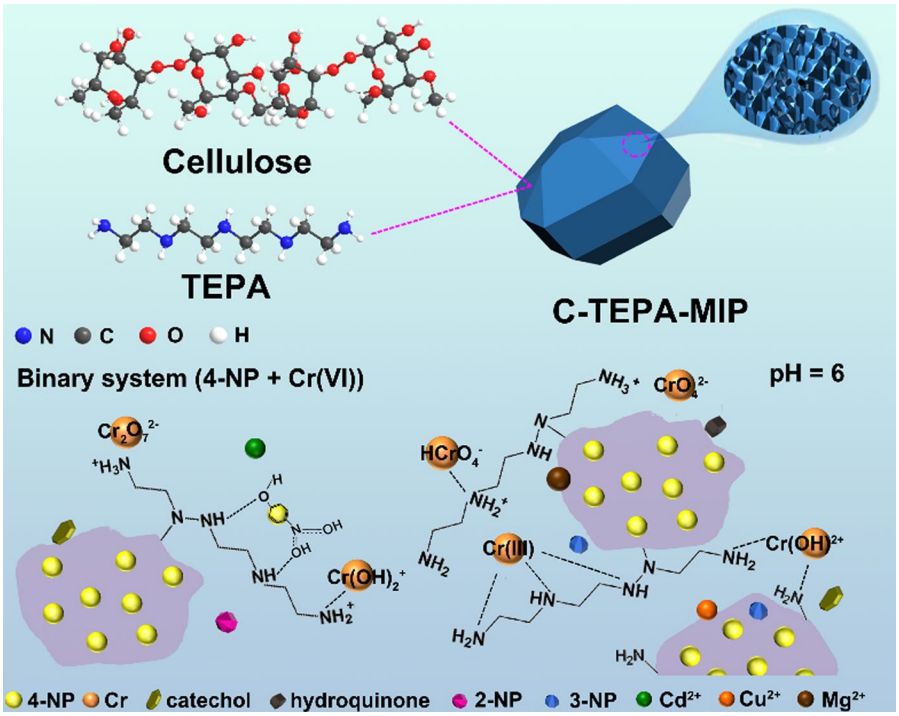

Keywords Cellulose · TEPA · Molecular imprinting polymer · Selective adsorption · 4-nitrophenol · Chromium (Cr)

Introduction

The global attention focused on environmental protection and renewable resources has made the search for multifunctional recyclable adsorption materials an urgent task. 4-nitrophenol (4-NP) and hexavalent chromium [Cr(VI)] are two of the most important pollutants of water. 4-NP is commonly used in chemical industry (Karami and Zeynizadeh 2019) and pharmaceuticals (Anh and Doong 2018). Cr(VI) is commonly used in electroplating, textiles, leather (Zhao et al. 2021a) and dyes (Guifang Wang et al. 2021). 4-NP and Cr(VI) are mutagenic, carcinogenic, highly toxic (Bahrami et al. 2020), and difficult to degrade. Thus, the low cost effective removal of 4-NP and Cr(VI) from the environment has become an important topic in the academic research and industrial applications (Chaleshtari and Foudazi 2020).

Molecular imprinting technology (MIT) is based on specific recognition between templates and molecularly imprinted polymers (MIPs). In MIT, the target molecule is polymerized with monomer or crosslinking agent to form a polymer, and then the template is removed to obtain MIPs. MIPs have the capacity to selectively adsorb the target molecule (BelBruno 2019; Schirhagl 2014), making MIT an effective solution for the challenges that arise from competitive adsorption (Cantarella et al. 2019; Mohammadi et al. 2021). An et al. (2019) designed and synthesized a series of surface molecularly imprinted polymers (SMIPs) using 2-nitrophenol (2-NP), 3-nitrophenol (3-NP), 4-NP and 4-methylphenol as templates, and applied them for the selective adsorption of phenols. Zhou et al. (2020) prepared a magnetic Cr(VI)-imprinted polymer using Fe_3O_4 nanoparticles as a carrier and $K_2Cr_2O_7$ as a template for removal of Cr(VI) in water. However, these adsorption materials (Kumar et al. 2020; Linye Jiang et al. 2016) are all monofunctional for either the organic pollutant 4-NP or the inorganic pollutant Cr(VI). It is

difficult to produce a dual-selective adsorbent using MIT for the two main reasons of (1) high consumption of monomers, and (2) reduction in the adsorption efficiency and adsorption capacity. More specifically, the presence of the two templates may cause a competitive reaction, in which one template occupies the imprinting site of the other template. Thus, challenges remain in the structural design of bifunctional adsorbents in MIPs, where the key question to be answered is how to avoid competitive adsorption in MIPs.

Tian et al. (2018) proposed a method to solve the competitive adsorption for the first time. The authors graphed poly(N-isopropylacrylamide) (PNIPAm) on graphene oxide (GO) and imprinted 4-NP as the template. The hydroxyl groups on the graphene could be used to adsorb lead [Pb(II)] ions, thus providing a means to fabricate a bifunctional adsorbent. This approach of obtaining a MIP using monomers that can bind to heavy metal ions might avoid the competitive adsorption, thus producing a bifunctional adsorbent for both organic and inorganic substances. A large number of studies have shown that nitrogen-containing adsorbents can adsorb Cr(VI) (Zhao et al. 2021b; Zhu et al. 2020). For example, Gao et al. (2020) prepared hollow spherical adsorbents using tannic acid (TA) and 1,6-hexanediamine (HA) and polyvinyl alcohol (PVA). The adsorption of Cr(VI) on the protonated amino groups was proved by X-ray photoelectron spectrometry (XPS). Xue et al. (2019) designed a cellulose-based solid amine adsorbent by crosslinking epichlorohydrin with microcrystalline cellulose (MCC) and tetraethylenepentamine (TEPA). Rathour et al. (2020) modified graphene oxide (GO) with ethylenediaminetetraacetic acid (EDTA), and used its amide bond to adsorb Cr(VI). The maximum adsorption capacity of EDTA@CO adsorbent for Cr(VI) was found to be 36.59 mg/g at pH 1.8.

Cellulose is one of the most popular natural polymers (Pereira et al. 2020), due to being abundantly available, cheap, ecofriendly, and biocompatible, and having characteristics such as high mechanical strength, and being easy to modify (Man et al. 2015; Ronglan Wu et al. 2015; Wu et al. 2015). The employment of cellulose as a carrier in MIPs could provide a solution for the recycling of the adsorbent. More specifically, the chain-like cellulose can be combined with other monomers and crosslinking agents to form a large-area imprinting layer, which increases imprinting sites and consequently improves the adsorption capacity. In addition, due to the good mechanical strength of cellulose, the damage of the imprinting sites can be prevented, which enhances the stability of the obtained adsorbent material.

In the present study, we aimed to synthesize a cellulose-based polymeric adsorbent (C-TEPA-MIP) selective for both 4-NP and Cr(VI). In order to achieve this goal, we used 4-NP as the template, TEPA as the monomer, and cellulose as the skeleton, where by graft polymerization, the polymer formed imprinted holes to selectively adsorb 4-NP. Cr(VI) was selectively adsorbed through the amine groups of TEPA monomer via coordination and electrostatic interactions. The C-TEPA-MIP exhibited the advantages of high adsorption performance and high selectivity, thus laying a foundation for the future development of adsorbents capable of the simultaneous adsorption of organic and inorganic pollutants.

Materials and methods

Materials

Cellulose (50 μm) was purchased from Hebei Balinway Superfine Materials Co., Ltd.; 1-allyl-methylimidazolium chloride (AMIMCl, ≥ 99%) from Moni Mooney Chemicals Co., Ltd.; 2-bromo-2-methylpropionyl bromide (≥ 97%), ethyleneglycol dimethacrylate (EGDMA, ≥ 98%) and N,N,N′,N″,N″-pentamethyldiethylenetriamine (PMDETA, ≥ 98%) from Aladdin Reagent Co., Ltd.; Cuprous(I) bromide (CuBr, ≥ 98%) from Across Chemical Co., Ltd.; tetraethylenepentamine (TEPA, ≥ 90%) from China Pharmaceutical Company; azodiisobutyronitrile (AIBN, ≥ 98%) from Chengdu Kelon Chemical Reagent Factory. AIBN was purified by recrystallization in methanol. Other reagents were purchased from Tianjin Hongyan Reagent Factory. Deionized water was used in all experiments.

Synthesis of cellulose-g-TEPA MIP (C-TEPA-MIP)

The synthesis route is shown in Scheme 1. Cellulose powder was dissolved in AMIMCl, and 2-bromo-2-methylpropionyl bromide was used to obtain bromine-terminated cellulose initiator. Afterwards, using 4-NP as the template, TEPA was grafted on

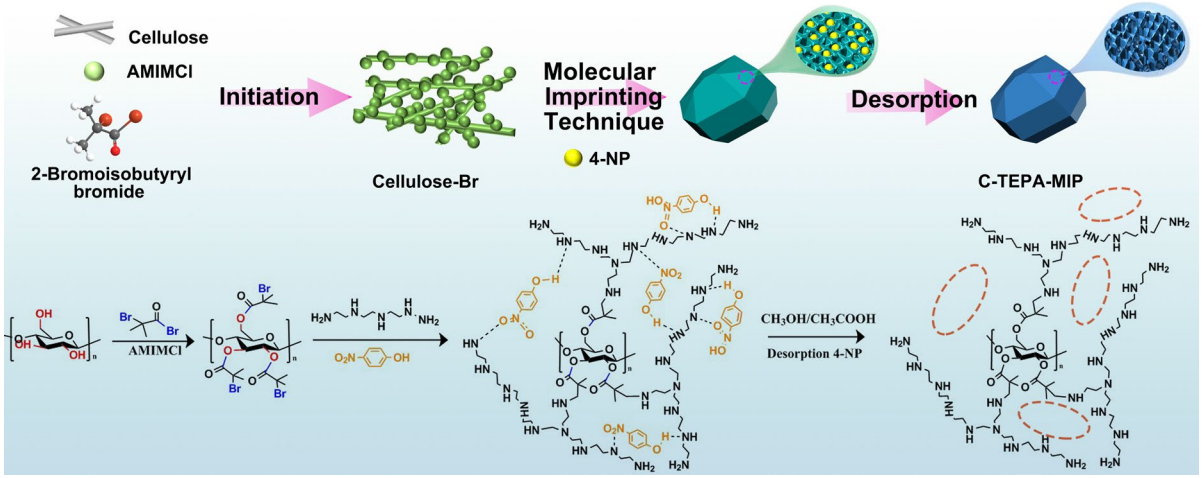

Scheme 1 The synthesis roadmap for obtaining C-TEPA-MIP

cellulose initiator to obtain cellulose-based polymer, and the imprinted polymer (i.e., C-TEPA-MIP) was obtained by desorption. For the synthesis, CuBr (7.75 mg), PMDETA (43.3 mg) and ascorbic acid (9.5 mg) were dissolved in N,N-Dimethylformamide (DMF) (100 mL). This solution is referred to as "DMF mixed solution" in the description of the later experiments.

Cellulose bromide (cellulose-Br) was synthesized according to our previous work (Lang et al. 2021). Cellulose-Br (50 mg) was dissolved in 3.75 mL of DMF mixed solution, and was further mixed with TEPA (0.568 g TEPA in 2 mL ethanol), 4-NP (41.7 mg), EGDMA (1.785 mL) and AIBN (16.4 mg), sequentially. For deoxygenation, the solution was purged with N_2 for 30 min. Polymerization of the solution was conducted for 24 h at 70 °C. After the completion of the polymerization, the polymer colloids were dialyzed for 3 days by changing water two times per day. The product was freeze-dried for 24 h. The product was eluted by methanol and acetic acid with a volume ratio of 9:1 until 4-NP could not be detected in the eluent. The product was subsequently washed by water until pH reached 7. The obtained powder sample was freeze-dried for 24 h, after which, it was subjected to a subsequent adsorption experiment and characterization. As a reference, the non-imprinted polymer (C-TEPA-NIP) was synthesized without adding 4-NP during the synthesis.

Effect of pH

Solutions containing 100 mg/L of 4-NP or Cr(VI) were prepared with pH in a range of 3–10. C-TEPA-MIP (10.0 mg) was added into each of these solutions together with 25 mL of 4-NP or Cr(VI) at different pH values. The pH was adjusted by 0.1 M NaOH or 0.1 M HCl solutions. The mixture was left for 12 h at 25 °C. Afterwards, the residual of 4-NP or Cr(VI) in the supernatant was determined by UV–Visible (UV-Vis) spectroscopy. A predetermined calibration curve was used for obtaining the concentration. For comparison, the same experiments were repeated for C-TEPA-NIP. All experiments were repeated 3 times to ensure reproducibility.

Equilibrium adsorption isotherm and kinetic study

The equilibrium adsorption isotherm and the kinetic of adsorption of 4-NP and Cr(VI) on C-TEPA-MIP and C-TEPA-NIP were studied. The results are provided in the Supplementary Information.

Selectivity of the adsorption

The selectivity study of the adsorption was carried out by comparing the adsorption capacities for 4-NP and Cr(VI) with those for other pollutants. For 4-NP, the comparison studies were conducted for 2-NP, 3-NP, catechol, and hydroquinone. In such experiments, C-TEPA-MIP or C-TEPA-NIP (10 mg) was added

to 25 mL solutions with the pollutants (100 mg/L). The adsorption lasted for 12 h at 25 °C. The pH of all solutions was 6. The concentrations of 4-NP, 3-NP, 2-NP, catechol, and hydroquinone were determined by UV–Vis spectroscopy at the wavelength of 317, 273, 278, 274 and 286 nm, respectively.

Similarly, a number of metal ions were chosen for the selective comparison studies for Cr(VI). These included Cu(II), Pb(II), Cd(II), Mg(II) and Zn(II). The experimental protocol and the conditions were the same as those for 4-NP, except that pH of the solution was 5 instead of 6. The concentrations of the inorganic metal ions were measured by atomic absorption spectrometer (AAS).

We also investigated the competitive adsorption in binary systems. The following pairs of co-existing pollutants were chosen: 4-NP/2-NP, 4-NP/3-NP, 4-NP/catechol, 4-NP/hydroquinone, Cr(VI)/Cu(II), Cr(VI)/Cd(II), and Cr(VI)/Zn(II). In the binary systems, the concentration of each pollutant was 50 mg/L, and the adsorption was conducted following the same protocol described above.

Recyclability of C-TEPA-MIP

For recycling C-TEPA-MIP and C-TEPA-NIP already used for adsorption experiments, the materials that adsorbed 4-NP were washed with a mixture of methanol and acetic acid (volume ratio of 9:1), and those that adsorbed Cr(VI) were washed with 0.1 M NaOH. Washing continued until 4-NP and Cr were not detected at 317 nm and 352 nm by UV–Vis spectroscopy, respectively. Afterwards, the materials were washed by deionized water to pH 7 and were freeze-dried to be used in the next adsorption experiment. This procedure signifies one adsorption–desorption cycle. The C-TEPA-MIP and C-TEPA-NIP were cyclically adsorbed for 7 times.

Characterization methods

The morphology of the materials was examined by scanning electron microscopy (SEM; SU8010, Hitachi, Japan) and transmission electron microscopy (TEM; FEI Tecnai G2 F20, America). Powder X-ray diffractometer (XRD; D8 Advance, Bruker AXS GmbH, Germany) was used to analyze the crystal form of the samples at 40 kV and 40 mA with Cu Kα radiation. Data were collected from 5° to 80° with a sampling interval of 0.02° per step and a scan speed of 10°/min. The chemical properties were characterized by Fourier transform infrared spectroscopy (FTIR; VERTEX 70, Bruker, Germany) using the KBr-disk method, where the spectra were recorded within the wavenumber of 500–4000 cm^{-1}. The elemental composition and the chemical state of the materials were characterized by XPS (Thermo Scientific K-Alpha, America). The pore size and the specific surface area of the materials were analyzed by accelerated surface area and porosimetry analysis (BET; ASAP2460, America). The surface charge of C-TEPA-MIP was measured by zeta potentiometer (Zeta; Nano ZS90, Malvern, America). The concentrations of 4-NP and Cr(VI) were determined by UV–visible spectroscopy (UV–Vis, UV1901PCS, Yoke, Shanghai). The concentrations of other metal ions were determined by AAS (240 AAS, Agilent, America).

Results and discussions

Morphology and structure determination

The morphology of C-TEPA-MIP (Fig. 1c, g) and C-TEPA-NIP (Fig. 1d, h) showed a reticular structure upon grafting of cellulose with TEPA, different from the microrods of the original cellulose (Fig. 1a, e) and cellulose-Br (Fig. 1b, f). The morphological features of C-TEPA-MIP and C-TEPA-NIP were similar. The morphologies of both of these materials were voluminous and had rough surfaces with partial pores (see Fig. 1c, d). The difference between the two structures concerned minor issues, where C-TEPA-MIP exhibited a smaller and more porous structure in comparison to C-TEPA-NIP. The special reticular pore structure of C-TEPA-MIP would facilitate the exposure of a higher number of active sites, which would play a conducive role during the adsorption process.

The physicochemical properties of the samples were characterized by FTIR and XRD. As shown in Fig. 1i, the FTIR spectra of cellulose and TEPA showed the characteristic peaks of cellulose and TEPA, including the characteristic broad peak of cellulose at 3349 cm^{-1} and the carbonyl (C=O) stretching vibration at 1721 cm^{-1} (Xu et al. 2019). For TEPA, the C–N vibration of C–NH–C at 1122 cm^{-1} and the vibration absorption peak of -NH_2 at 1463 cm^{-1} were observed (Xue et al. 2019). The peak

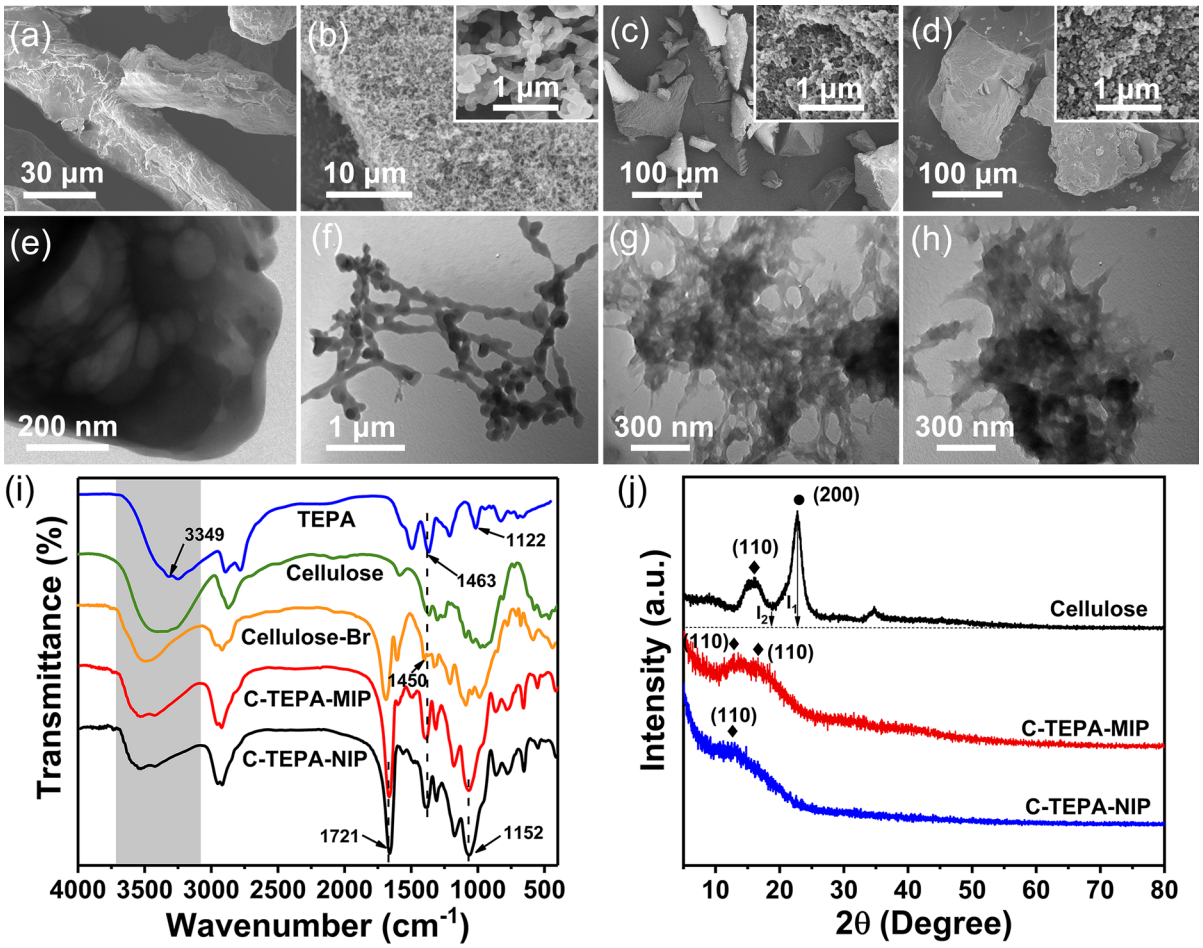

Fig. 1 SEM and TEM micrographs of **a**, **e** cellulose, **b**, **f** cellulose-Br, **c**, **g** C-TEPA-MIP, and **d**, **h** C-TEPA-NIP. **i** FTIR spectra of the materials. **j** XRD patterns of cellulose, C-TEPA-MIP and C-TEPA-MIP

at 1450 cm^{-1} was assigned to -$C(CH_3)_3$ stretching of 2-bromo-2-methylpropionyl bromide. Both C-TEPA-MIP and C-TEPA-MIP exhibited the characteristic absorption peaks of cellulose and TEPA, where only the C–N adsorption peak was shifted to 1152 cm^{-1}. The FTIR analysis indicated that cellulose-Br was successfully prepared, and TEPA was successfully grafted onto cellulose. Meanwhile, the XRD patterns in Fig. 1j indicated the presence of two main characteristic peaks at $2\theta = 16.6°$ and 23.2° corresponding to (110) and (200) reflections of cellulose, respectively (Kumari and Chauhan 2014). In addition, the crystallinity of cellulose was calculated to be 80% based on the intensity (I_1) at 23° and the intensity (I_2) at 18° (Kljun et al. 2011). In the XRD patterns of C-TEPA-MIP and C-TEPA-NIP, the (110) reflection of cellulose was shifted and broadened and its (200) reflection disappeared. By using 4-NP as the template and/or grafting of TEPA, the new interactions formed within the material between TEPA fragments, 4-NP or cellulose resulted in the disruption of the original crystalline order of cellulose to a large extent. This provides indirect evidence for the success of TEPA grafting and 4-NP imprinting processes applied to cellulose.

The optimization of materials preparation

Adsorption capacity of MIPs is highly dependent on the synthetic conditions employed, including the amounts of the monomer TEPA, the crosslinking agent EGDMA, and the template molecule 4-NP.

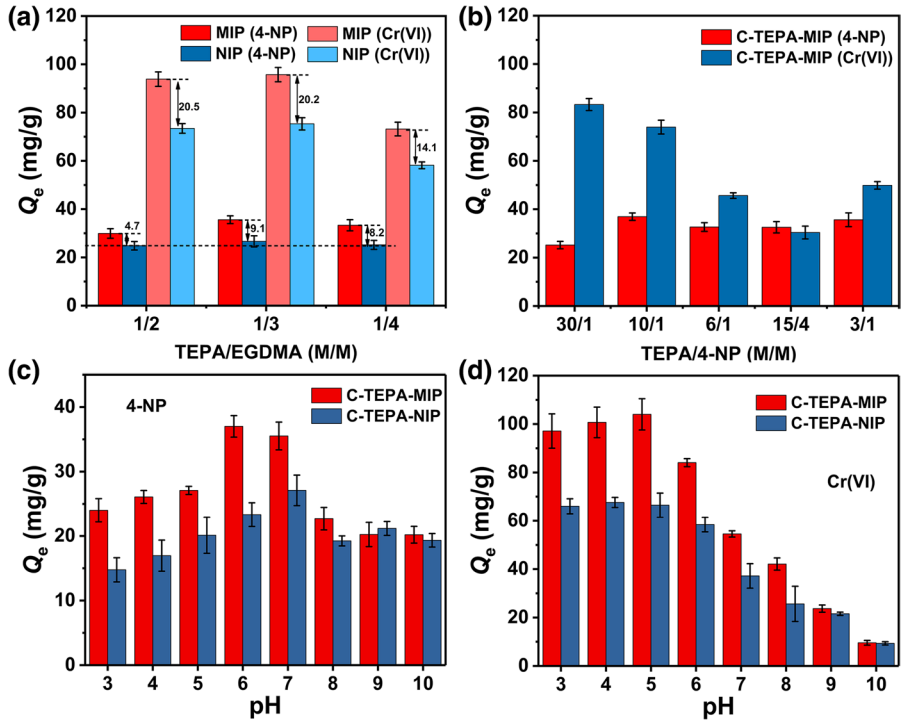

Fig. 2 Influence of the molar ratio of **a** TEPA/EGDMA and **b** TEPA/4-NP on the adsorption capacity of C-TEPA-MIP. The effect of pH variation on the equilibrium adsorption capacity (Q_e) of C-TEPA-MIP and C-TEPA-NIP for **c** 4-NP and **d** Cr(VI)

For optimizing the performance of C-TEPA-MIP, the effect of the molar ratio of the monomer on the crosslinker was investigated (Fig. 2a). For 4-NP, when the ratio of TEPA/EGDMA decreased, the adsorption capacity of MIP and NIP first increased and then decreased. The adsorbed amount reached the maximum when TEPA/EGDMA was 1/3. However, the increase for NIP was smaller or unchanged in comparison to that for MIP, indicating that TEPA had a certain effect on the adsorption of MIP, but had a negligible effect on the adsorption of NIP. For 4-NP, the maximum difference of adsorption capacity between MIP and NIP was 9.1 mg/g when TEPA/EGDMA was 1/3. This result indicates that neither a low nor a high monomer content is beneficial to the adsorption of 4-NP, which can be explained as follows. A small amount of TEPA induces a small number of TEPA-formed cavities, which results in a low adsorbed amount of 4-NP. On the other hand, for a too large amount of TEPA, the MIP layer becomes so thick that access to the internal imprinted cavities becomes difficult, thus imposing a limit on the adsorption of 4-NP. For Cr(VI), the adsorption capacity decreased significantly when TEPA/EGDMA was 1/4, which indicates that the adsorption of Cr(VI) mainly depends on the TEPA content. It is also reasonable to suspect that the exposure of TEPA could be an influential factor. Coincidentally, the highest adsorption capacity for both 4-NP and Cr(VI) was found at the ratio of TEPA/EGDMA = 1/3.

The choice of the template is also a crucial factor in the preparation of imprinted polymers, because it determines the number of imprinted cavities. In Fig. 2b, upon a decrease in TEPA/4-NP molar ratio, the adsorption capacity of C-TEPA-MIP for 4-NP first increased, then decreased and stabilized. The maximum adsorption capacity occurred at the TEPA/4-NP molar ratio of 10/1. The occurrence of a stabilized adsorption capacity could be explained by the low amount of TEPA, which imposed a limitation on the formation of 4-NP imprinting cavities. The adsorption of Cr(VI) on C-TEPA-MIP was decreased once TEPA/4-NP molar ratio decreased. Therefore, in the experiments that followed, the molar ratios of TEPA/EGDMA and TEPA/4-NP were set to 1/3 and 10/1, respectively.

The effect of pH on adsorption capacity

The pH under which the adsorption occurs significantly affects the adsorption capacity of the adsorbent for organic pollutants and heavy metals. Thus, we assessed the effects of pH variation on the adsorption of 4-NP and Cr(VI) by C-TEPA-MIP and C-TEPA-NIP. The equilibrium adsorption capacity (Q_e) of C-TEPA-MIP was higher than that of C-TEPA-NIP at all pH values (Fig. 2c, d). The adsorption capacity of C-TEPA-MIP for 4-NP first increased and then decreased once pH varied in the range 3–10, where the maximum of Q_e (37.01 mg/g) was reached at pH 6 (see Fig. 2c). The same trend was observed for Cr(VI), where the maximum of Q_e (104.13 mg/g) occurred at pH 5 (Fig. 2d). These results can be explained by the effects that arise from the employed synthetic procedure. More specifically, the imprinting process was carried out in an organic solvent, where both TEPA and 4-NP molecules were in the non-ionized states. Therefore, the specific adsorption of 4-NP should be best realized under the condition that 4-NP and TEPA are predominantly uncharged, i.e., for 4-NP when $pH < pK_a$ (7.15) and for TEPA with the lowest number of charged units ($pK_{a1} = 9.68$; $pK_{a2} = 9.10$; $pK_{a3} = 8.08$; $pK_{a4} = 4.72$; $pK_{a5} = 2.98$). Thus, it is no surprise that the maximum Q_e occurred at pH 6 for 4-NP. At low pH, the effect of imprinting on adsorption was evident, where the difference of the adsorption between C-TEPA-MIP and C-TEPA-NIP was indicative of the template-specific adsorption brought about by the imprinted cavities.

Cr(VI) mainly exists in the forms of $Cr_2O_7^{2-}$ and $HCrO_4^-$ in water (Zuo et al. 2020), which explains why C-TEPA-MIP and C-TEPA-NIP exhibited the highest degree of equilibrium adsorption capacity for Cr(VI) at low pH values. More specifically, because the surface of C-TEPA-MIP was positively charged in an acidic condition, the closer the pH of the media to the neutral, the higher was the positive potential of the C-TEPA-MIP surface. The maximum positive potential occurred at pH 6. In an alkaline condition, the surface of C-TEPA-MIP was negatively charged (see Fig. 3). The amine groups on C-TEPA-MIP were protonated under the acidic condition, which generated amine cations that could adsorb negatively charged pollutants through electrostatic interactions. However, as pH increased the amine groups in TEPA became deprotonated, and consequently the surface positive charge of the adsorbent decreased, thus inducing a reduction in the adsorption capacity for Cr(VI). Remarkably, the adsorption of Cr(VI) by C-TEPA-MIP was better in comparison with C-TEPA-NIP, which may be due to the existence of imprinted pores, which resulted in a higher degree of exposure for the active sites. This is consistent with what was found in pH-varying adsorption experiments discussed above.

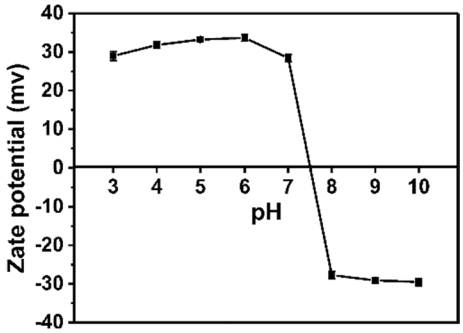

Fig. 3 Zeta potential of the C-TEPA-MIP as a function of pH

Adsorption isotherm and kinetics of adsorption

Through the study of adsorption kinetics (Fig. S1 and Table S1) and thermodynamics (Fig. S2 and Table S2), it was found that the adsorption models of C-TEPA-MIP for 4-NP and Cr(VI) were in accordance with pseudo-second-order kinetics and Langmuir isothermal model. In the solution of 800 mg/L 4-NP and 600 mg/L Cr(VI), the maximum adsorption capacities of C-TEPA-MIP for 4-NP and Cr(VI) were 126.34 mg/g and 136.75 mg/g, respectively, which were higher than those of C-TEPA-NIP (Table S2).

Selective adsorption

The selective adsorption of 4-NP and Cr(VI) on the adsorbents was investigated in both unitary and binary systems. Among the five structurally identical phenols (Fig. 4a), C-TEPA-MIP adsorbed more nitrophenols than catechol and resorcinol, where the largest adsorption was for 4-NP. The adsorption of 4-NP on C-TEPA-MIP was obviously higher than that on C-TEPA-NIP. In the other four phenolic compounds, the difference between adsorption by C-TEPA-MIP

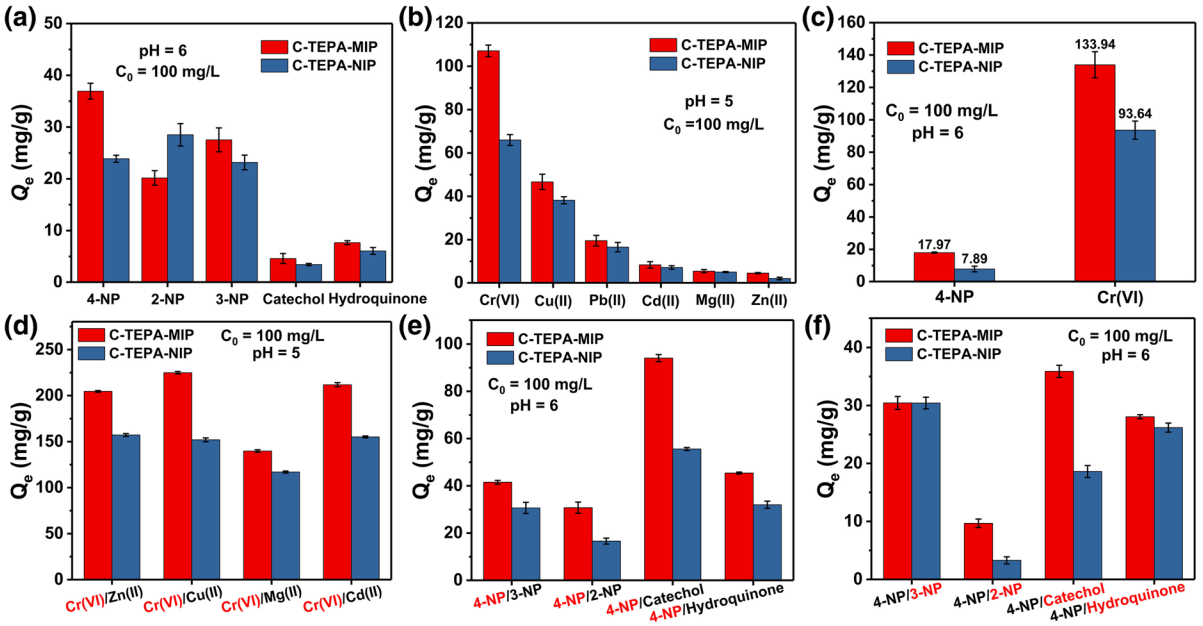

Fig. 4 Adsorption capacity of C-TEPA-MIP and C-TEPA-NIP in single component solutions of **a** different phenols, and **b** different metal ions, and in binary solutions containing **c** 4-nitrophenol and Cr(VI) [Q_e for both 4-NP and Cr(VI)], **d** Cr(VI) and other metal ions [Q_e for Cr(VI)], **e** 4-NP and other phenols (Q_e for 4-NP), **f** 4-NP and other phenols (Q_e for other phenols)

and C-TEPA-NIP was not obvious, which could be explained by the similarity of the imprinting pore cavities that was induced by the similarity in the structures of 3-NP, 2-NP and 4-NP. The nitrogen atom and the oxygen atoms of phenols will form hydrogen bonds through interactions with the hydrogen atoms of the adsorbents, and their phenol-group hydrogen atoms will form hydrogen bonding with the nitrogen atoms of TEPA. Thus, C-TEPA-MIP showed different adsorption effects for the five phenols investigated. The selective adsorption of Cr(VI) by C-TEPA-MIP is shown in Fig. 4b, where it was found that the adsorption of Cr(VI) by C-TEPA-MIP was maximal, due to the role played by the amine groups of TEPA in the adsorption process.

In order to demonstrate the selectivity of adsorption, competitive adsorption tests were carried out in binary system as described in the Materials and Methods. In all of the cases (Fig. 4c–f), C-TEPA-MIP adsorbed more pollutants than C-TEPA-NIP. In the solution containing both 4-NP and Cr(VI) (Fig. 4c), the adsorption capacities for these two pollutants exhibited a large difference. Also, the adsorption capacities of C-TEPA-MIP for Cr(VI) and 4-NP were higher than those of C-TEAP-NIP. Co-existence of Cr(VI) with other metal ions induced an interference in its adsorption, resulting in different adsorption capacities for Cr(VI) in the presence of different co-existing metal ions (Fig. 4d). For example, for both C-TEPA-MIP and C-TEPA-NIP, the adsorption of Cr(VI) was the strongest in the Cr(VI)/Cu(II) system and was the weakest in the Cr(VI)/Mg(II) system. In binary 4-NP/interfering phenol systems, the adsorption of 4-NP on the adsorbent was significantly stronger than the adsorption of other phenols (Fig. 4e, f).

In order to elucidate the selectivity of C-TEPA-MIP, the distribution coefficients (K_d) of 4-NP and Cr(VI) in the binary mixtures were calculated by Eq. (1) (Qu et al. 2020).

$$K_d = \frac{Q_e}{C_e} \tag{1}$$

In Fig. 5a, c, the K_d values of C-TEPA-MIP and C-TEPA-NIP exhibited the highest degree of difference in the unitary solution of 4-NP and Cr(VI), whereas little differences were observed in the solutions that contained catechol, hydroquinone and other heavy metal ions. In their binary systems (Fig. 5b, d),

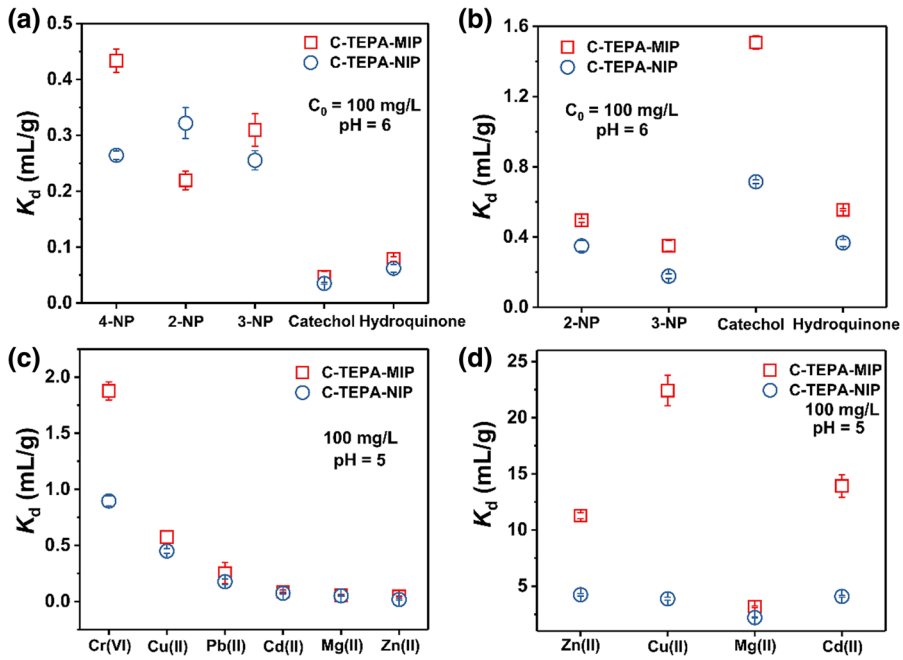

Fig. 5 The K_d values of C-TEPA-MIP and C-TEPA-NIP for phenols in **a** unitary and **b** binary systems. The K_d values of C-TEPA-MIP and C-TEPA-NIP for heavy metal ions in **c** unitary and **d** binary systems

the K_d values of the two polymers for 4-NP showed certain degrees of differences, where the highest degree of difference in K_d was observed in the 4-NP/catechol solution. For the K_d values of Cr(VI), large differences were observed in the binary mixtures, except for the Cr(VI)/Mg(II) system. These indicate that C-TEPA-MIP exhibited a selective adsorption and higher affinity for the organic pollutant 4-NP and the inorganic metal ion Cr(VI).

We compared our results with those found in the literature for the adsorbents for 4-NP and Cr(VI) (Table 1). Due to the importance of pH in the adsorption process, in Table 1 we have mainly cited 4-NP adsorbents with pH 6 and Cr(VI) adsorbents with pH 5. Comparisons made between our results and other entries of Table 1 revealed that in most of the cases our C-TEPA-MIP adsorbent showed superior adsorption capacity and selectivity for 4-NP and Cr(VI).

Desorption and recycling of C-TEPA-MIP

Efficiency of recycling is an important index in the economical evaluation of an adsorbent. Thus, the pot life and cycle efficiency of C-TEPA-MIP and C-TEPA-NIP adsorbents were evaluated. The adsorption capacity of C-TEPA-MIP for 4-NP exhibited a slight change in the first six cycles (Fig. 6a), where the adsorption efficiency was reduced to 92.28% (Fig. 6c). In the seventh cycle, the adsorption capacity reduced to 84.15%. In comparison to C-TEPA-MIP, the adsorption capacity and efficiency of C-TEPA-NIP for 4-NP had a slight change in the first seven cycles. This might be due to (1) the detachment of MIP from the adsorbent upon solvent washing, and (2) the presence of non-removed 4-NP in the adsorbent that could not elute during solvent washing. These factors may affect the next cycle of adsorption, thus inducing a reduction in the adsorption capacity. Reductions were observed in the adsorption capacity and efficiency of C-TEPA-MIP for Cr(VI) (Fig. 6b, d). One may expect that this adsorbent could not be recycled for Cr(VI), because after the first cycle, the adsorption capacity was halved and the adsorption efficiency decreased to 58.24% in the second cycle. Nevertheless, after the second cycle up to the seventh one, the adsorption capacity decreased slowly. The latter happened, because the adsorption of Cr(VI) on the adsorbent is dependent on the amine group of TEPA, meaning that upon the first adsorption, almost all of the amine groups were capable of making complexes with Cr(VI) or forming hydrogen bonding, thus inducing the adsorption of Cr(VI). Because of this strong binding mode, not all Cr(VI) ions could be removed during washing with solvent. This affected

Table 1 Comparison between the adsorption capacity of C-TEPA-MIP and some previously reported adsorbents for 4-NP and Cr(VI)

Adsorbent	Capacity for 4-NP (mg/g)	Capacity for Cr(VI) (mg/g)	pH
C-TEPA-MIP (this study)[a]	181.82	134.41	6; 5
Surface-immobilized 4-NP-MMIP (Mehdinia et al. 2014)[a]	129.1	–	5
N-(2-aminoethyl)-3-(trimethoxysilyl)propylamine surface modified potassium tetratitanate whisker–MIP (Guan et al. 2011)[a]	22.11	–	6
4-NP-MMIP (Mehdinia et al. 2013)[a]	57.8	–	5
Fe_3O_4@SiO_2 @4-NP-SMIP (Liang et al. 2020)[a]	134.23	–	7
Cr-erephthalic acidv (Chen et al. 2017)[b]	19	–	6
Polymeric calix arene-tethered silica (Dogan et al. 2020)[b]	2.3	–	5
Pure grapheme (Ismail 2015)[b]	15.5	–	6
MIP-macromolecule polyethyleneimine/SiO_2 (An et al. 2012)[b]	155.5	–	7
Aminopropyl-modified MCM-48 (Gu et al. 2018)[b]	107.53	–	6.5
Silver(I) 3,5-diphenyltriazolate MOF (Miao et al. 2020)[b]	48.4	–	7
Bis(dodecyldimethylammonio)-2-butane dibromide/organo–vermiculites (Yu et al. 2018)[b]	106.5	–	6
Microalgal biochars (Zheng et al. 2017)[b]	204.8	–	7
Reduced graphene oxide hydrogel-combined-magnetic metal–organic frameworks (Mohamed 2021)[b]	288.36	197.28	6; 2
Microcrystalline cellulose/TEPAA (Xue et al. 2019)[b]	–	327	4
Acid-activated kaolinite (Gupta 2006)[b]	–	8.0	4.6
Copolymer-templated nitrogen-doped carbons (Song et al. 2018)[b]	–	17.2	5
Cationic (carboxymethyl) trimethylammonium chloride hydrazide modified cellulose (Huang et al. 2020b)[b]	–	80.5	6
Aniline-co-5-sulfo-2-anisidine/Fe_3O_4 (Huang et al. 2020a)[b]	–	213.6	5
Aniline/Fe_3O_4 (Huang et al. 2020a)[b]	–	136.1	5
Methoxyaniline/Fe_3O_4 (Huang et al. 2020a)[b]	–	126.7	5
Chitosan/polypyrrole composite (Janmohammadi et al. 2021)[b]	–	78.61	4.2
N-methylimidazolium function alized strongly basic anion exchange resins in the Cl^- (Lili Zhu and Chen 2009)[b]	–	132	4.6
N-methylimidazolium function alized strongly basic anion exchange resins in the SO_4^{2-} (Lili Zhu and Chen 2009)[b]	–	125	4.6
Micro-sized goethite@activated carbon (Su et al. 2019)[b]	–	27.2	5.6

[a]The adsorbent is selective for the contaminants

[b]The adsorbent is not selective for the contaminants

the adsorption efficiency of the second cycle, where a reduction of 41.76% efficiency was observed. It is noteworthy that the adsorption efficiency of the seventh cycle was only 29.29% (of the first cycle) lower than that of the second cycle. In order to find out the reason why the adsorption capacity decreased with the number of cycles, FTIR and XRD measurements were carried out on the adsorbent before and after each recycling.

The FTIR spectra of C-TEPA-MIP exhibited little changes before and after adsorbing 4-NP and Cr(VI) (Fig. 7a). The minor changes observed concerned slight changes in the characteristic peaks of asymmetric and symmetric nitro group (-NO_2) at 1589 and 1344 cm^{-1}, respectively, and the characteristic peak of the aromatic ring at 753 cm^{-1}. The latter indicated that 4-NP was adsorbed on the adsorbent. In addition, the characteristic IR absorption peak of potassium dichromate appeared at 884 cm^{-1}, which indicated that Cr(VI) was also in the adsorbent. Conversely, the XRD patterns of C-TEPA-MIPs that were subjected to adsorption changed, which indicated changes in the

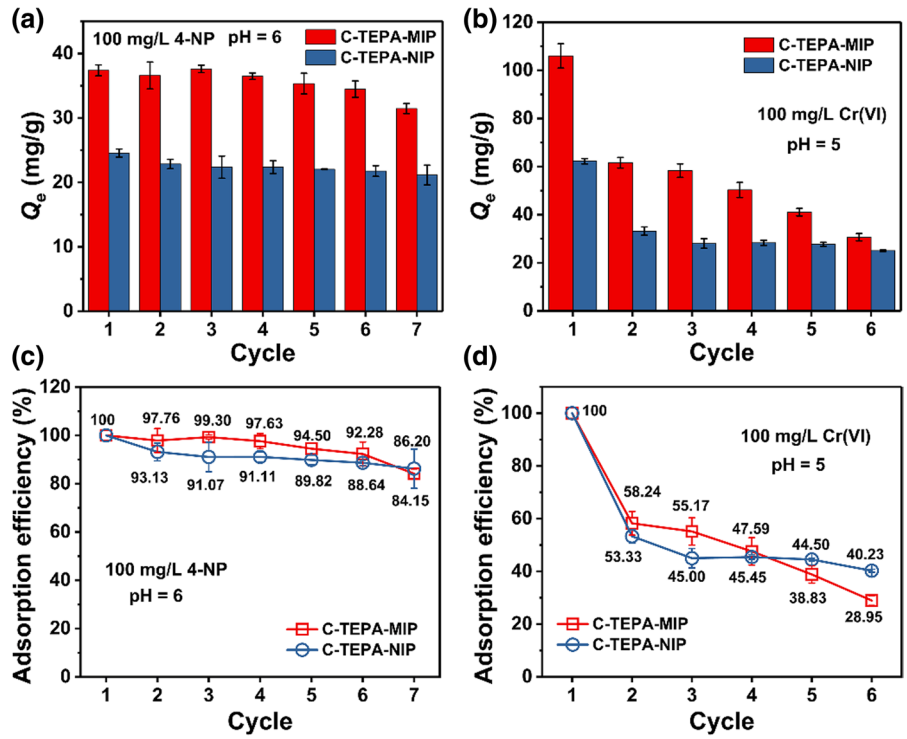

Fig. 6 Adsorption capacity after each recycling for **a** 4-NP and **b** Cr(VI). Adsorption efficiency after each recycling for **c** 4-NP and **d** Cr(VI)

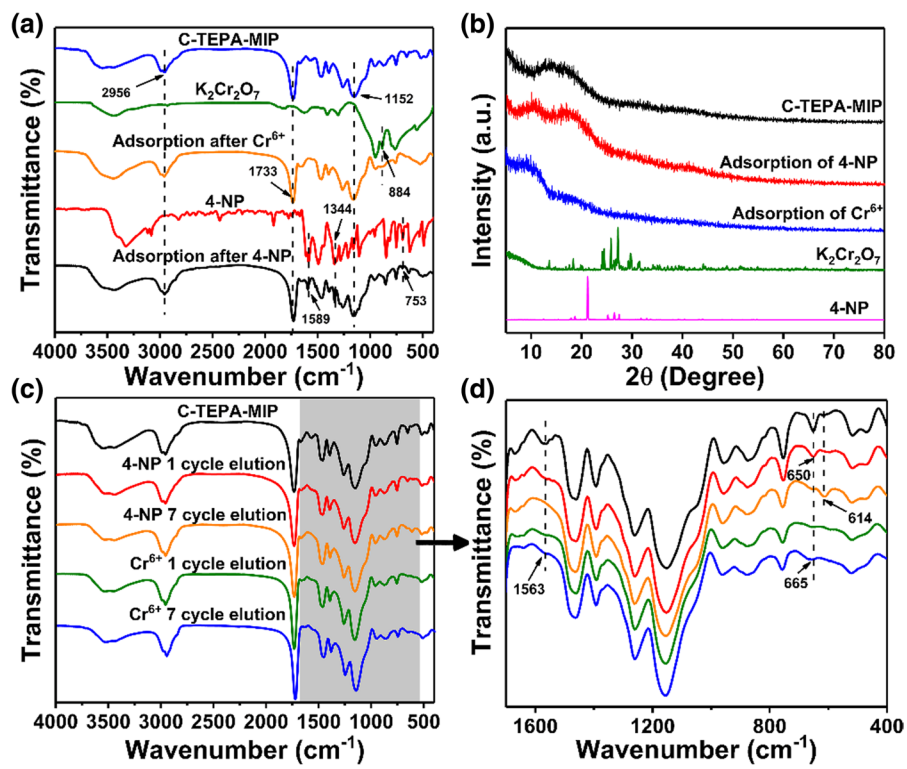

Fig. 7 **a** Infrared diagram of C-TEPA-MIP, $K_2Cr_2O_7$, 4-NP, adsorbed 4-NP and C-TEPA-MIP adsorb Cr(VI). **b** XRD pattern of C-TEPA-MIP, $K_2Cr_2O_7$, 4-NP, 4-NP adsorbed and C-TEPA-MIP adsorb Cr(VI). **c** Infrared patterns of eluted C-TEPA-MIP subjected to the 1st and the 7th adsorptions of 4-NP and Cr(VI). **d** Enlargement of c

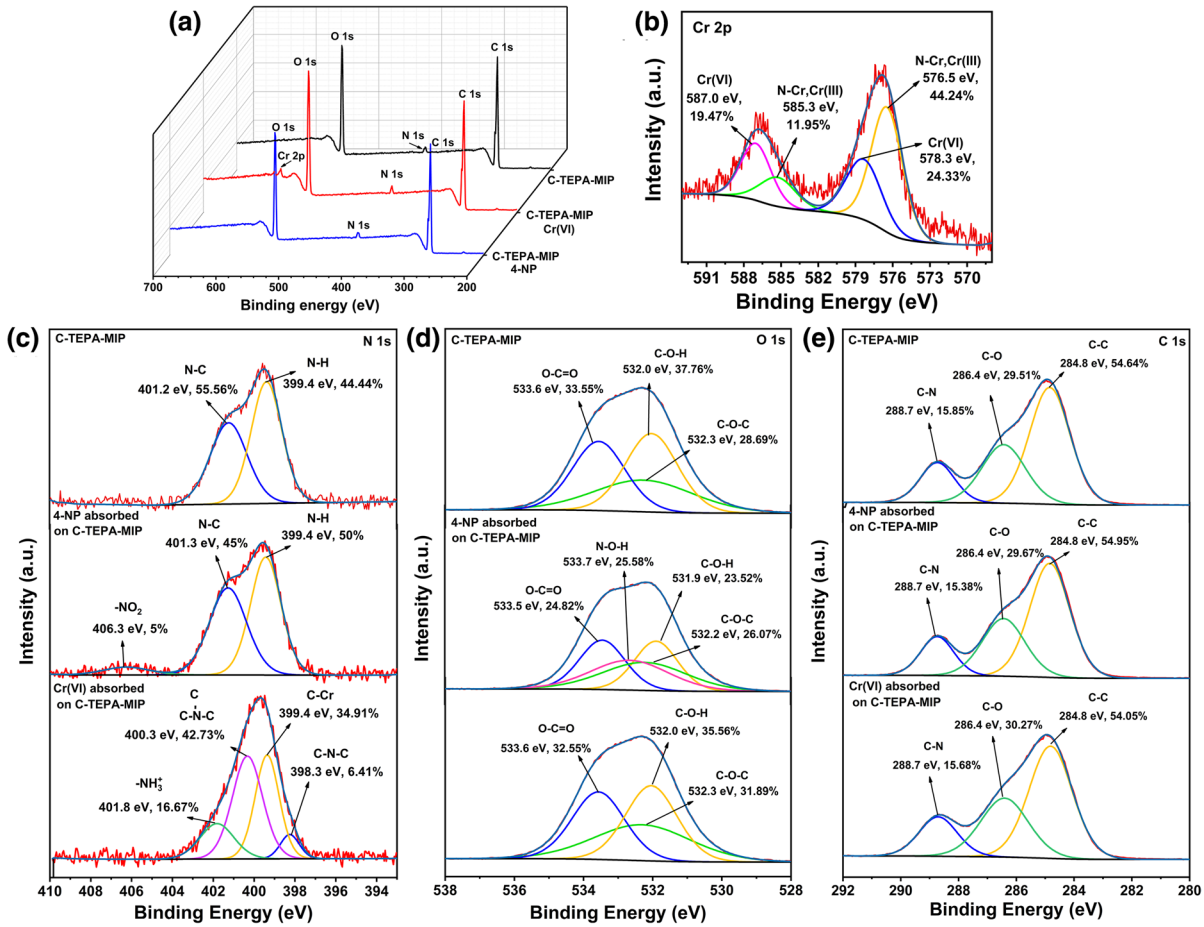

Fig. 8 **a** XPS spectra of 4-NP and Cr(VI) adsorbed on C-TEPA-MIP. **b** Cr 2p spectrum of C-TEPA-MIP after adsorbing Cr(VI). For different materials, **c** N 1s, **d** O 1s, and **e** C 1s spectra

crystalline structures (Fig. 7b). In addition, we compared the IR spectra of elution after the 1st and the 7th cycles (Fig. 7c, d). Figure 7d shows the magnified spectra of the grey area in Fig. 7c. The structure of C-TEPA-MIP changed slightly after recycling. For 4-NP, upon the 7th adsorption, the absorption peaks of N–H bond stretching vibration (1563 cm^{-1}) and C–H bond plane bending vibration (650 cm^{-1}) of the eluted adsorbent subjected to the 1st adsorption disappeared and became smaller, respectively. The absorption of C–H bond at 614 cm^{-1} became larger, indicating that the number of nitrogen atoms that could form hydrogen bonding with 4-NP was reduced, thus inducing a reduction in the adsorption performance of the adsorbent. For Cr(VI), the FTIR data revealed similarities with that of 4-NP cycle, where the difference lied in two aspects. First, upon the 7th adsorption, the vibration of the C–N bond at 650 cm^{-1} shifted to 665 cm^{-1}. Second, the peak intensity of C–N bond decreased. These indicated that there were fewer nitrogen atoms on the adsorbent, which resulted in fewer lone pair electrons that could interact with Cr, thus inducing reductions in the adsorption capacity and the cycle efficiency of the adsorbent (Luo et al. 2020).

In order to shed light on the molecular structure of the adsorbent, as well as the characteristics of the adsorption of 4-NP and Cr(VI) on C-TEPA-MIP, XPS analysis was carried out for the adsorbent before and after adsorption. In the survey spectrum (Fig. 8a), the peaks of the O 1s, C 1s, N 1s and Cr 2p orbitals were identified. In Cr 2p spectrum (Fig. 8b), the adsorption of Cr(VI) on C-TEPA-MIP had two main binding forms, one was N–Cr(III) at 576.5 eV and 585.3 eV,

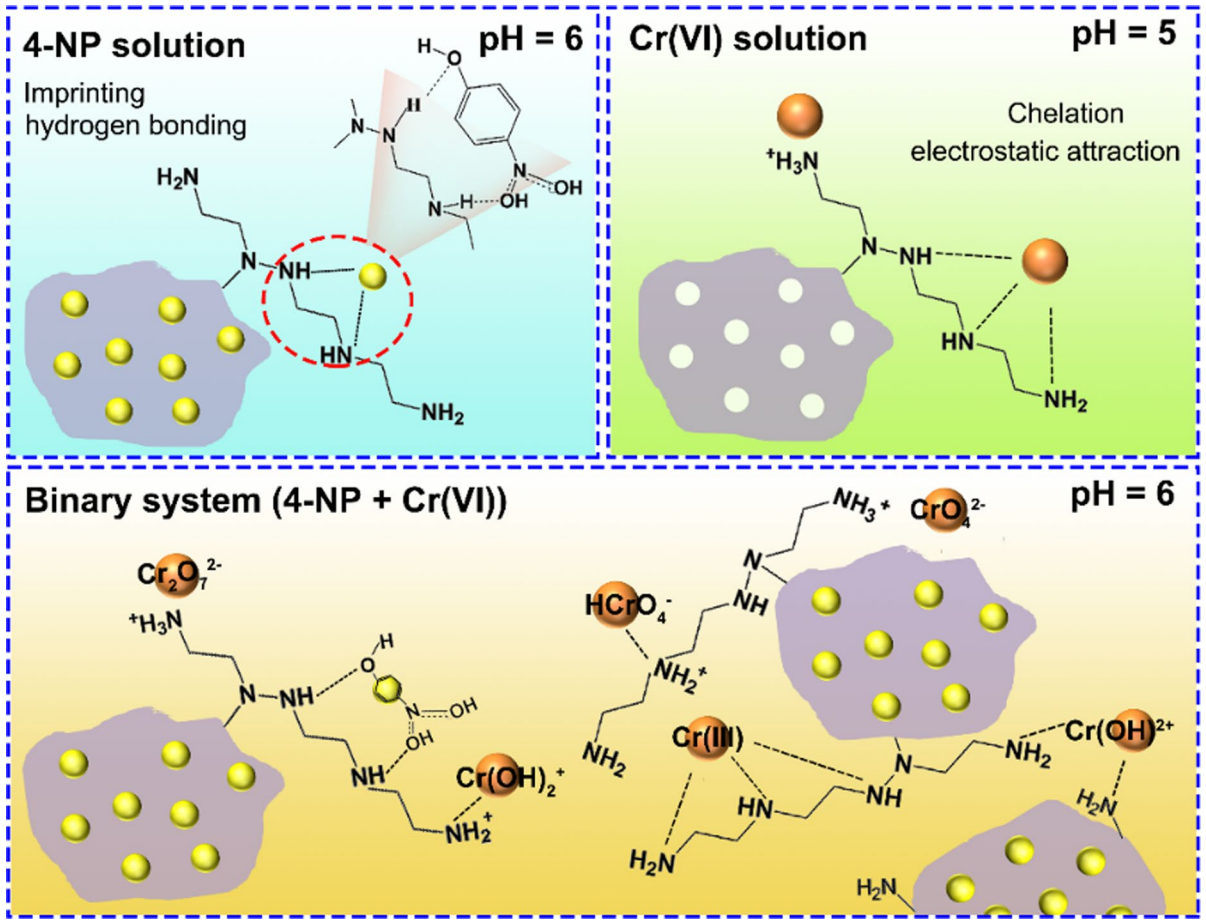

Fig. 9 Illustration of the adsorption process of 4-NP and Cr(VI) on C-TEPA-MIP

and the other was Cr(VI) at 578.3 eV and 587.0 eV (Guo et al. 2020) This happened, because after adsorption of Cr(VI), part of Cr(VI) was reduced to Cr(III), and potassium dichromate was converted to $HCrO_4^-$ and $Cr_2O_7^{2-}$ [Eqs. (10) and (11)] under acidic conditions, meaning that $HCrO_4^-$ and $Cr_2O_7^{2-}$ were the dominant ions. Because upon adsorption chromium was combined with nitrogen, we also analyzed the N 1s of C-TEPA-MIP after adsorbing Cr(VI). In Fig. 8c, it is observed that the two peaks of N1s of C-TEPA-MIP at 401.2 eV and 399.4 eV were $N(CH_3)_3$ and N–H, respectively. After adsorption of Cr(VI), the peak of $N(CH_3)_3$ shifted to 400.3 eV. In addition, two new peaks of 399.4 eV (N–Cr) and 401.8 eV ($-NH_3^+$) were observed on the N 1s spectrum of C-TEPA-MIP after adsorbing Cr(VI). These further illustrate that the amine groups of TEPA (-NH-, -N=, and $-NH_2$) participated in the adsorption of Cr(VI) through electrostatic interactions and coordination. Thus, they became protonated under the acidic condition to chelate with Cr (He et al. 2020) [see Eq. (2), (3), (4), (5) and (6)]. In these equations, the $-NH_2$ group is taken as an example, and electrostatically bind to negatively charged Cr [see Eq. (7) and (8)].

$$Cr_2O_7^{2-} + H_2O \rightarrow HCrO_4^- + H^+ \quad (2)$$

$$HCrO_4^- \rightleftharpoons Cr_2O_4^{2-} + H^+ \quad (3)$$

$$-NH_2 + Cr(OH)^{2+} \rightarrow -NH_2Cr(OH)^{2+} \quad (4)$$

$$-NH_2 + Cr(OH)_2^+ \rightarrow -NH_2Cr(OH)_2^+ \quad (5)$$

$$-NH_2 + Cr^{3+} \rightarrow -NH_2Cr^{3+} \quad (6)$$

$$-NH_3^+ + HCrO_4^- \rightarrow NH_3^+ - HCrO_4^- \quad (7)$$

$$-NH_3^+ + Cr_2O_7^{2-} \rightarrow NH_3^+ - Cr_2O_7^{2-} \quad (8)$$

In the adsorption of 4-NP, the only major difference observed between XPS data of the adsorbent before the adsorption and after it was the addition of the 406.3 eV peak of the -NO_2 group (Shong et al. 2016). A minor difference also existed, which comprised of the observation that the ratio of N–H bonds was 6% higher after the adsorption compared to that observed before the adsorption, indicating that the adsorption of 4-NP onto the adsorbent occurred through imprinting and hydrogen bonding between N and H. In the spectra of O 1s (Fig. 8d) and C 1s (Fig. 8e), in addition to the O 1s spectrum of C-TEPA-MIP after 4-NP adsorption, there is an additional peak of N–O–H bond at 533.7 eV, which is the free hydroxyl group of 4-NP assigned to a single NO_2 cycloaddition product (Shong et al. 2016), resulting in different proportions of O–C=O, C–O–H and C–O–C bonds in O 1s of C-TEPA-MIP after 4-NP adsorption. The peak positions and proportions of other peaks in the spectra of O 1s and C 1s before and after the adsorption were close to each other. The values of the parameters of the specific surface area, the pore radius and the pore volume are listed in Table S2. The values of the specific surface areas of C-TEPA-MIP, C-TEPA-MIP adsorbing 4-NP and C-TEPA-MIP adsorbing Cr(VI) were 118.090 m^2/g, 107.711 m^2/g and 171.734 m^2/g. Combined analysis of data of Table S3 and Fig. S3 revealed that (1) the specific surface area of C-TEPA-MIP after adsorption of 4-NP was smaller than that observed before adsorption, whereas the specific surface area of C-TEPA-MIP after adsorption of Cr(VI) was larger than that determined before adsorption, and (2) the radius of the pores of C-TEPA-MIP did not change before and after adsorption of Cr(VI) and remained 1.48 nm. Thus, it is concluded that (1) upon the adsorption of 4-NP the imprinting chambers inside the adsorbent were occupied, resulting in a smaller surface area for C-TEPA-MIP, and (2) the adsorption of Cr(VI) occurred on the surface of the adsorbent, which increased its the specific surface area. In short, the adsorption of 4-NP occurred on the inside of the adsorbent and relied on the internal imprinting cavity and, in part, on the hydrogen bonding capability, whereas the adsorption of Cr(VI) mainly happened on the TEPA surface of the polymer and was dependent on the complexation of amine groups and electrostatic attraction. Thus, the two pollutants did not compete for occupying the adsorption sites. The illustration of the adsorption process is shown in Fig. 9.

Conclusion

In this paper, a novel type of cellulose-based adsorbent with bifunctional selectivity for 4NP and Cr(VI) was successfully synthesized. During the synthesis process, TEPA was grafted and polymerized onto the cellulose framework and 4-NP played the role of the template. During the adsorption process, 4-NP was adsorbed by imprinted sites and hydrogen bonding, and Cr(VI) was adsorbed by the electrostatic attraction and chelation between nitrogen atoms of the monomer (i.e., TEPA) and Cr(VI). The experimental results showed that the maximum equilibrium adsorption capacity of C-TEPA-MIP for 4-NP was 126.34 mg/g and for Cr(VI) was 136.75 mg/g. The adsorption of the two compounds on the adsorbent followed the Langmuir isothermal model and the pseudo-second-order kinetic model. The competitive adsorption also showed high selectivity for 4-NP and Cr(VI). It was noteworthy that the adsorption efficiency of 4-NP on the adsorbent was still above 90% after six cycles of adsorption–desorption.

Acknowledgments This research was financially supported by the National Natural Science Foundation of China (No. 21868036, and No. 32061133005) and the Tianshan Youth Program (No. 2020Q011). Language editing by Hermes Editing is acknowledged. The authors would like to thank the workers in Shiyanjia Lab (https://www.shiyanjia.com) for SEM, TEM, XPS and BET tests.

Funding Open access funding provided by University of Bergen (incl Haukeland University Hospital).

Declarations

Conflict of interest The authors declare that they have no conflict of interest.

Human and animal rights This research does not contain any studies with humans or animals as subjects.

References

An F-Q, Li H-F, Guo X-D, Hu T-P, Gao B-J, Gao J-F (2019) Design of novel "imprinting synchronized with crosslinking" surface imprinted technique and its application for selectively removing phenols from aqueous solution. Eur Polym J 112:273–282. https://doi.org/10.1016/j.eurpolymj.2019.01.015

An FQ, Gao BJ, Feng XQ (2012) Binding and recognition ability of molecularly imprinted polymer toward p-nitrophenol. J Appl Polym Sci 125:2549–2555. https://doi.org/10.1002/app.36403

Anh NTN, Doong R-a (2018) One-step synthesis of size-tunable gold@sulfur-doped graphene quantum dot nanocomposites for highly selective and sensitive detection of nanomolar 4-nitrophenol in aqueous solutions with complex matrix. ACS Appl Nano Mater 1:2153–2163. https://doi.org/10.1021/acsanm.8b00210

Bahrami S, Yaftian MR, Najvak P, Dolatyari L, Shayani-Jam H, Kolev SD (2020) PVDF-HFP based polymer inclusion membranes containing Cyphos® IL 101 and Aliquat® 336 for the removal of Cr(VI) from sulfate solutions. Sep Purif Technol 250:117251. https://doi.org/10.1016/j.seppur.2020.117251

BelBruno JJ (2019) Molecularly imprinted polymers. Chem Rev 119:94–119. https://doi.org/10.1021/acs.chemrev.8b00171

Cantarella M, Carroccio SC, Dattilo S, Avolio R, Castaldo R, Puglisi C, Privitera V (2019) Molecularly imprinted polymer for selective adsorption of diclofenac from contaminated water. Chem Eng J 367:180–188. https://doi.org/10.1016/j.cej.2019.02.146

Chaleshtari ZA, Foudazi R (2020) Polypyrrole@polyHIPE composites for hexavalent chromium removal from water. ACS Appl Polym Mater 2:3196–3204. https://doi.org/10.1021/acsapm.0c00362

Chen J, Sun X, Lin L, Dong X, He Y (2017) Adsorption removal of o-nitrophenol and p-nitrophenol from wastewater by metal-organic framework Cr-BDC. Chinese J Chem Eng 25:775–781. https://doi.org/10.1016/j.cjche.2016.10.014

Dogan M, Temel F, Tabakci M (2020) High-performance adsorption of 4-nitrophenol onto calix[6]arene-tethered silica from aqueous solutions. J Inorg Organomet P 30:4191–4202. https://doi.org/10.1007/s10904-020-01571-0

Gao S, Liu Q, Liu Q, Yuan C, Gao T, Yao J (2020) Facile synthesis of hollow globular Cr(VI)-adsorbents inspired from assembly to polymerization. J Clean Prod 250:119485. https://doi.org/10.1016/j.jclepro.2019.119485

Gu X, Kang H, Li H, Liu X, Dong F, Fu M, Chen J (2018) Adsorption removal of various nitrophenols in aqueous solution by aminopropyl-modified mesoporous MCM-48. J Chem Eng Data 63:3606–3614. https://doi.org/10.1021/acs.jced.8b00477

Guan W, Pan J, Wang X, Hu W, Xu L, Zou X, Li C (2011) Selective recognition of 4-nitrophenol from aqueous solution by molecularly imprinted polymers with functionalized tetratitanate whisker composites as support. J Sep Sci 34:1244–1252. https://doi.org/10.1002/jssc.201100032

Guifang Wang HX, Zhu J, Zhao H, Liu K, Ma S, Zhang S, Komarneni S (2021) Simultaneous removal of Zn^{2+} and p-nitrophenol from wastewater using nanocomposites of montmorillonite with alkyl-ammonium and complexant. Environ Res 201:111496. https://doi.org/10.1016/j.envres.2021.111496

Guo X et al (2020) Adsorption mechanism of hexavalent chromium on biochar: kinetic, thermodynamic, and characterization studies. ACS Omega 5:27323–27331. https://doi.org/10.1021/acsomega.0c03652

Gupta KGBaSS, (2006) Adsorption of chromium (VI) from water by clays. Ind Eng Chem Res 45:7232–7240. https://doi.org/10.1021/ie060586j

He PY, Zhang YJ, Chen H, Han ZC, Liu LC (2020) Low-cost and facile synthesis of geopolymer-zeolite composite membrane for chromium(VI) separation from aqueous solution. J Hazard Mmater 392:122359. https://doi.org/10.1016/j.jhazmat.2020.122359

Huang Q-S, Wang C, Wei W, Ni B-J (2020a) Magnetic poly(aniline-co-5-sulfo-2-anisidine) as multifunctional adsorbent for highly effective co-removal of aqueous Cr(VI) and 2,4-Dichlophenol. Chem Eng J 387:124152. https://doi.org/10.1016/j.cej.2020.124152

Huang X, Dognani G, Hadi P, Yang M, Job AE, Hsiao BS (2020b) Cationic dialdehyde nanocellulose from sugarcane bagasse for efficient chromium (VI) removal. ACS Sustain Chem Eng 8:4734–4744. https://doi.org/10.1021/acssuschemeng.9b06683

Ismail AI (2015) Thermodynamic and kinetic properties of the adsorption of 4-nitrophenol on graphene from aqueous solution. Can J Chem 93:1083–1087. https://doi.org/10.1139/cjc-2014-0450

Janmohammadi M, Baghdadi M, Adyel TM, Mehrdadi N (2021) Waste plastic filter modified with polyaniline and polypyrrole nanoparticles for hexavalent chromium removal. Sci Total Environ 752:141850. https://doi.org/10.1016/j.scitotenv.2020.141850

Karami S, Zeynizadeh B (2019) Reduction of 4-nitrophenol by a disused adsorbent: EDA-functionalized magnetic cellulose nanocomposite after the removal of Cu(2). Carbohydr

Polym 211:298–307. https://doi.org/10.1016/j.carbpol.2019.01.113

Kljun A, Benians TA, Goubet F, Meulewaeter F, Knox JP, Blackburn RS (2011) Comparative analysis of crystallinity changes in cellulose I polymers using ATR-FTIR, X-ray diffraction, and carbohydrate-binding module probes. Biomacromolecules 12:4121–4126. https://doi.org/10.1021/bm201176m

Kumar S et al (2020) Fabrication of chromium-imprinted polymer: a real magneto-selective sorbent for the removal of Cr(vi) ions in real water samples. New J Chem 44:18668–18678. https://doi.org/10.1039/d0nj04054a

Kumari S, Chauhan GS (2014) New cellulose-lysine schiff-base-based sensor-adsorbent for mercury ions. ACS Appl Mater Interfaces 6:5908–5917. https://doi.org/10.1021/am500820n

Lang D et al (2021) DMAEMA-grafted cellulose as an imprinted adsorbent for the selective adsorption of 4-nitrophenol. Cellulose 28:6481–6498. https://doi.org/10.1007/s10570-021-03920-9

Liang W, Lu Y, Li N, Li H, Zhu F (2020) Microwave-assisted synthesis of magnetic surface molecular imprinted polymer for adsorption and solid phase extraction of 4-nitrophenol in wastewater. Microchem J 159:105316. https://doi.org/10.1016/j.microc.2020.105316

Lili Zhu YL, Chen Ji (2009) Synthesis of N-methylimidazolium functionalized strongly basic anion exchange resins for adsorption of Cr(VI). Ind Eng Chem Res 48:3261–3267. https://doi.org/10.1021/ie801278f

Linye Jiang HL, Li M, Xing Y, Ren X (2016) Surface molecular imprinting on CdTe quantum dots for fluorescent sensing of 4-nitrophenol. Anal Methods-UK 8:2226–2232. https://doi.org/10.1039/C5AY03160E

Luo Z, Guo M, Jiang H, Geng W, Wei W, Lian Z (2020) Plasma polymerization mediated construction of surface ion-imprinted polypropylene fibers for the selective adsorption of Cr(VI). React Funct Polym 150:104552. https://doi.org/10.1016/j.reactfunctpolym.2020.104552

Man X, Wu R, Jiang X, Xu S, Wang W (2015) Organo-montmorillonite supported titania nanocomposite synthesized by using poly(methyl methacrylate) grafted cellulose as template and its application in photodegradation. Cellulose 22:3189–3198. https://doi.org/10.1007/s10570-015-0704-1

Mehdinia A, Baradaran Kayyal T, Jabbari A, Aziz-Zanjani MO, Ziaei E (2013) Magnetic molecularly imprinted nanoparticles based on grafting polymerization for selective detection of 4-nitrophenol in aqueous samples. J Chromatogr A 1283:82–88. https://doi.org/10.1016/j.chroma.2013.01.093

Mehdinia A, Dadkhah S, Baradaran Kayyal T, Jabbari A (2014) Design of a surface-immobilized 4-nitrophenol molecularly imprinted polymer via pre-grafting amino functional materials on magnetic nanoparticles. J Chromatogr A 1364:12–19. https://doi.org/10.1016/j.chroma.2014.08.058

Miao H, Song S, Chen H, Zhang W, Han R, Yang G (2020) Adsorption study of p-nitrophenol on a silver (I) triazolate MOF. J Porous Mat 27:1409–1417. https://doi.org/10.1007/s10934-020-00917-w

Mohamed AK (2021) Magnetic metal-organic frameworks embedded in a reduced graphene oxide hydrogel network as a promising hybrid nanocomposite for Cr(VI) and p-nitrophenol removal. J Chem Eng Data 66:2929. https://doi.org/10.1021/acs.jced.0c00890

Mohammadi R, Hezarjaribi M, Ramasamy DL, Sillanpää M, Pihlajamäki A (2021) Application of a novel biochar adsorbent and membrane to the selective separation of phosphate from phosphate-rich wastewaters. Chem Eng J 407:126494. https://doi.org/10.1016/j.cej.2020.126494

Pereira ALS, Feitosa JPA, Morais JPS, Rosa MF (2020) Bacterial cellulose aerogels: Influence of oxidation and silanization on mechanical and absorption properties. Carbohydr Polym 250:116927. https://doi.org/10.1016/j.carbpol.2020.116927

Qu Y, Qin L, Liu X, Yang Y (2020) Reasonable design and sifting of microporous carbon nanosphere-based surface molecularly imprinted polymer for selective removal of phenol from wastewater. Chemosphere 251:126376. https://doi.org/10.1016/j.chemosphere.2020.126376

Rathour RKS, Bhattacharya J, Mukherjee A (2020) Selective and multicycle removal of Cr(VI) by graphene oxide–EDTA composite: Insight into the removal mechanism and ionic interference in binary and ternary associations. Environ Technol Inno 19:100851. https://doi.org/10.1016/j.eti.2020.100851

Ronglan Wu LT, Wang W, Man X (2015) Bifunctional cellulose derivatives for the removal of heavy-metal ions and phenols: Synthesis and adsorption studies. J Appl Polym Sci. https://doi.org/10.1002/app.41830

Schirhagl R (2014) Bioapplications for molecularly imprinted polymers. Anal Chem 86:250–261. https://doi.org/10.1021/ac401251j

Shong B, Hellstern TR, Bent SF (2016) Adsorption of heterobifunctional 4-nitrophenol on the Ge(100)-2 × 1 surface. Surf Sci 650:279–284. https://doi.org/10.1016/j.susc.2015.04.007

Song Y et al (2018) Copolymer-templated synthesis of nitrogen-doped mesoporous carbons for enhanced adsorption of hexavalent chromium and uranium. ACS Appl Nano Mater 1:2536–2543. https://doi.org/10.1021/acsanm.8b00103

Su M et al (2019) Enhanced hexavalent chromium removal by activated carbon modified with micro-sized goethite using a facile impregnation method. Sci Total Environ 647:47–56. https://doi.org/10.1016/j.scitotenv.2018.07.372

Tian L et al (2018) A novel GO/PNIPAm hybrid with two functional domains can simultaneously effectively adsorb and recover valuable organic and inorganic resources. Chem Eng J 343:607–618. https://doi.org/10.1016/j.cej.2018.03.015

Wu R, Tian L, Wang W (2015) Synthesis of a nanocomposite of organo-montmorillonite/cellulose-g-poly(methyl methacrylate) by atom-transfer radical polymerization and its application in removal of 2,4-dichlorophenol. Cellulose 22:3633–3643. https://doi.org/10.1007/s10570-015-0751-7

Xu X et al (2019) Preparation and characterization of cellulose grafted with epoxidized soybean oil aerogels for oil-absorbing materials. J Agric Food Chem 67:637–643. https://doi.org/10.1021/acs.jafc.8b05161

Xue F, He H, Zhu H, Huang H, Wu Q, Wang S (2019) Structural design of a cellulose-based solid amine adsorbent for the complete removal and colorimetric detection of Cr(VI). Langmuir 35:12636–12646. https://doi.org/10.1021/acs.langmuir.9b01788

Yu M, Gao M, Shen T, Wang J (2018) Organo-vermiculites modified by low-dosage Gemini surfactants with different spacers for adsorption toward p-nitrophenol. Colloid Surf A 553:601–611. https://doi.org/10.1016/j.colsurfa.2018.05.095

Zhao J, Boada R, Cibin G, Palet C (2021a) Enhancement of selective adsorption of Cr species via modification of pine biomass. Sci Total Environ 756:143816. https://doi.org/10.1016/j.scitotenv.2020.143816

Zhao N et al (2021b) Microscopic mechanism about the selective adsorption of Cr(VI) from salt solution on O-rich and N-rich biochars. J Hazard Mater 404:124162. https://doi.org/10.1016/j.jhazmat.2020.124162

Zheng H et al (2017) Adsorption of p-nitrophenols (PNP) on microalgal biochar: Analysis of high adsorption capacity and mechanism. Bioresource Technol 244:1456–1464. https://doi.org/10.1016/j.biortech.2017.05.025

Zhou Z et al (2020) Preparation of highly efficient ion-imprinted polymers with Fe_3O_4 nanoparticles as carrier for removal of Cr(VI) from aqueous solution. Sci Total Environ 699:134334. https://doi.org/10.1016/j.scitotenv.2019.134334

Zhu D et al (2020) Highly efficient and selective removal of Cr(VI) by covalent organic frameworks: Structure, performance and mechanism. Colloid Surf A 600:124910. https://doi.org/10.1016/j.colsurfa.2020.124910

Zuo K et al (2020) A Hybrid metal-organic framework-reduced graphene oxide nanomaterial for selective removal of chromate from water in an electrochemical process. Environ Sci Technol 54:13322–13332. https://doi.org/10.1021/acs.est.0c04703